GeoHealth

RESEARCH ARTICLE

10.1029/2024GH001283

Effects of Ozone-Depleting Substances on Ultraviolet Radiation and Skin Cancer Rates in Australia and the United States of America

Julia Lee-Taylor[1], Zeyu Hu[1], Jessica Kyle[1], Ken Karipidis[2], Stuart Henderson[2], Robert Landolfi[3], Christopher M. Tasich[3], and Sasha Madronich[1]

[1]ICF, Arlington, VA, USA, [2]Australian Radiation Protection and Nuclear Safety Agency, Yallambie, VIC, Australia, [3]United States Environmental Protection Agency, Washington, DC, USA

Key Points:

- Population-weighted clear-sky UV doses are 24% higher in Australia than in the USA, mainly because Australians live closer to the equator
- Differences in population-weighted UV doses are too small to explain larger incidence rates of UV-related maladies in Australia than the USA
- Human-caused stratospheric ozone depletion raised incidence rates by <1% for melanoma and <5% for squamous cell carcinoma in both countries

Correspondence to:

J. Kyle,
jessica.kyle@icf.com

Citation:

Lee-Taylor, J., Hu, Z., Kyle, J., Karipidis, K., Henderson, S., Landolfi, R., et al. (2026). Effects of ozone-depleting substances on ultraviolet radiation and skin cancer rates in Australia and the United States of America. *GeoHealth*, *10*, e2024GH001283. https://doi.org/10.1029/2024GH001283

Received 30 MAY 2025
Accepted 16 JAN 2026

Author Contributions:

Conceptualization: Julia Lee-Taylor, Zeyu Hu, Stuart Henderson, Robert Landolfi, Sasha Madronich
Data curation: Julia Lee-Taylor, Zeyu Hu, Ken Karipidis, Christopher M. Tasich
Formal analysis: Julia Lee-Taylor, Zeyu Hu, Ken Karipidis, Sasha Madronich
Investigation: Julia Lee-Taylor, Zeyu Hu, Stuart Henderson, Sasha Madronich
Methodology: Julia Lee-Taylor
Project administration: Jessica Kyle, Robert Landolfi, Christopher M. Tasich

Abstract Stratospheric ozone (O_3) losses and consequent increases in surface ultraviolet (UV) radiation remain a health concern due to close association with skin cancers and cataracts. This study estimated how emissions of ozone-depleting substances (ODS) affect, via O_3 reductions, surface UV radiation and associated health impacts in Australia compared to the United States. We used climatological atmospheric data and the U.S. Environmental Protection Agency's Atmospheric Health Effects Framework (AHEF) model to estimate these effects for historic and projected ODS emissions. Compared to the United States, the Australian population is potentially exposed to ca. 24% more biologically weighted UV radiation because of the closer proximity of its population to the equator, less stratospheric O_3 at comparable latitudes, and seasonal variations in the Earth-Sun distance. Surface UV increments owing to ODS-caused stratospheric O_3 depletion were largest in the 1990s, while the estimated health impacts peak several decades later at ca. 0.5% for cataracts, 1% for melanoma incidence, and 5% for keratinocyte cancer incidence (relative to 1980), and are similar in both countries. The study found that differences in population-weighted surface UV can only partly explain Australia's substantially higher incidence and mortality rates for UV-related maladies. Other factors like genetic susceptibility of skin types, exposure behaviors, and diagnosis practices likely play a role.

Plain Language Summary Ozone in the upper atmosphere helps block harmful ultraviolet (UV) radiation from reaching Earth's surface. Chemicals known as ozone-depleting substances (ODS) can reduce ozone levels, allowing more UV radiation through. Increased UV exposure increases the risk of health problems like skin cancer and cataracts. The amount of UV that reaches the surface varies by location. In this study, we used a model to compare UV exposure and resulting skin cancer and cataract rates between the United States and Australia. Australians receive about 24% more harmful UV radiation under clear skies. Our study explains that this is due mostly to Australia's closer proximity to the equator, and partly due to climatological differences in stratospheric ozone and seasonal variations in the Earth-Sun distance. We further estimate that ozone depletion has increased incidence rates of UV-induced illness similarly in both Australia and the USA, and by less than 5 percent. Overall, the study found that differences in UV radiation only partly explain the significantly higher rates of UV-induced illness in Australia than in the USA, suggesting that other factors like genetic susceptibility of skin types, exposure behaviors, and diagnosis practices likely play a role.

1. Introduction

Skin cancer and cataract are widespread health problems associated with exposure to environmental ultraviolet (UV) radiation (Neale et al., 2023). Globally, annual premature deaths were estimated to be ca. 57,000 from cutaneous malignant melanoma in the year 2020 (Arnold et al., 2022), and ca. 56,000 from keratinocyte cancers in the year 2019 (Zhang et al., 2021). Approximately 6.7 million disability-adjusted life years (DALYs) were lost due to cataract in 2019 (Löfgren, 2017). Incidence rates vary greatly between and within countries due to differences in genetic, cultural, and economic backgrounds and geographic variations in UV radiation levels.

The amount of UV radiation reaching the Earth's surface varies strongly with location and time. While some variations are known with astronomical precision (e.g., the variation during the solar year in the Earth's distance from the Sun, or the Sun's daily path across the sky) others, such as clouds, pollutants, and atmospheric ozone (O_3), are less predictable and potentially sensitive to human activities. Concerns about stratospheric O_3 depletion have led over the past several decades to a much better understanding of ground-level UV radiation, via direct

Software: Julia Lee-Taylor
Visualization: Julia Lee-Taylor, Ken Karipidis, Sasha Madronich
Writing – original draft: Julia Lee-Taylor, Zeyu Hu, Sasha Madronich
Writing – review & editing: Julia Lee-Taylor, Zeyu Hu, Jessica Kyle, Ken Karipidis, Stuart Henderson, Robert Landolfi, Christopher M. Tasich, Sasha Madronich

observations from ground-based stations (reviewed by Bernhard et al. (2023)) and less directly though with greater geographic coverage from satellite-based observations (Arola et al., 2009; Herman et al., 2020; Lee-Taylor et al., 2010). An international environmental treaty, the Montreal Protocol on Substances that Deplete the Ozone Layer (Montreal Protocol) with its amendments and adjustments, has phased out the production of most ozone-depleting substances (ODS) worldwide (UNEP, 2020), avoiding future scenarios in which ODS would deplete stratospheric O_3 to a fraction of current values (Newman et al., 2009). Such catastrophic O_3 depletion would in turn have caused several-fold increases in ground-level UV radiation (McKenzie et al., 2019) and adverse health effects (Madronich et al., 2021; van Dijk et al., 2013). As a result of the Montreal Protocol, changes in stratospheric O_3 over populated areas have been relatively small over the past few decades, and will likely remain so, although their future sign and magnitude remain uncertain and scenario dependent (WMO, 2022).

In addition to environmental UV radiation, many other factors are likely to be involved in the epidemiology of skin cancers and cataracts, such as genetics and behavior. Both the United States (USA) and Australia have robust registry data for these UV-related diseases. This presents an opportunity to estimate how ozone depletion could impact environmental UV radiation and these diseases' incidence in the two countries. Incidence rates for these maladies are generally much higher in Australia, but it is unclear how much of this can be reasonably attributed to differences in the UV environment.

This study uses climatological atmospheric data and numerical models to estimate the differences in UV exposures experienced by the population of the two countries, the contribution of ODS to long-term changes in these exposures, and the implications for cancer and cataract incidence. We employ the Atmospheric Health Effects Framework (AHEF) model (U.S. EPA, 2020), a numerical model developed and used by the U.S. Environmental Protection Agency (EPA) to estimate the adverse health impacts of changing ODS emissions in the USA (Madronich et al., 2021). The model computes geographic differences in UV radiation and applies those to the respective population distributions and baseline incidences, allowing estimation of changes in disease due to past or future UV radiation variations. The model specifically allows estimation of the adverse effects attributable to the depletion of O_3 by ODS emissions that have already occurred over the past four decades.

2. Methods

2.1. Model Overview

The AHEF model is used by the EPA to evaluate changes in human health effects associated with a depleted stratospheric ozone layer. It estimates the number of skin cancer and cataract cases and deaths from skin cancer in the USA that will be prevented by protecting the ozone layer, which results in a decrease of the UV radiation reaching the Earth's surface that causes these diseases. The model was described in detail by U.S. EPA (2020) and by Madronich et al. (2021) (henceforth M21) and was applied in the latter study to the USA to evaluate the benefits of the phaseout of ODS by the Montreal Protocol, compared to their unabated growth (the so-called "world avoided" scenario).

In brief, the model consists of a series of five sub-models that connect ODS emissions scenarios to their UV-related human health impacts. The sub-models in turn: (a) describe historical and projected ODS emissions; (b) calculate the associated stratospheric chlorine loading and O_3 changes from a pre-ozone-depletion baseline (usually defined as the year 1980); (c) calculate the consequent changes in ground-level biologically weighted UV irradiance; (d) calculate cumulative UV exposure by age at specific latitudes; and (e) combine the UV projections with observed dose-response relationships, health registry data, and population projections to quantify the changes in the rates of health effects relative to the baseline year and resulting from the specified ODS emissions.

For the current study, we specify annual ODS emissions according to the World Meteorological Organization (WMO) A1 emissions scenario (WMO, 2018), which remains in common use, for example, in the most recent Scientific Assessment Panel (SAP) report on O_3 depletion (WMO, 2022). The A1 scenario reasonably represents historical to present emission values, and its future scenario follows expectations of continued compliance with the Montreal Protocol. The model combines these with atmospheric transport times and the relative ozone depletion potential of different ODS molecules to estimate stratospheric halogen loading (Equivalent Effective Stratospheric Chlorine, EESC), and then uses satellite-observed correlations between EESC and stratospheric O_3 from 1979 to 1990 (McPeters et al., 1996) to estimate stratospheric O_3 depletion as a function of the ODS

concentrations. The O_3-filtered UV radiation reaching the Earth's surface is estimated from look-up tables generated with the Tropospheric Ultraviolet Visible (TUV) model (Lee-Taylor & Madronich, 2007; Madronich, 1987). The spectral irradiance is integrated with a biological weighting function (action spectrum) based on laboratory studies of skin cancer induction in mice, corrected for the transmission spectrum of human skin (de Gruijl et al., 1993), and for cortical cataract on studies of cataract induction in pig lenses (Oriowo et al., 2001). Cumulative lifetime UV radiation exposures are calculated for each population cohort alive during the study period, then finally used to estimate changes in malady incidences and mortality from those reported by public health records. While the AHEF was originally developed to estimate health impacts due to stratospheric change on the U.S. population, we adapted the model to the Australian context for the purposes of this study, as described below.

2.2. Earth-Sun Distance

In AHEF, the monthly mean Earth-Sun distance (ESD) is computed with an algorithm based on the Astronomical Almanac (Michalsky, 1988). This is necessary because the amount of solar radiation reaching Earth is inversely proportional to the square of this distance and is ca. 6.9% stronger in early January (perihelion) compared to early July (aphelion). Averaged over the year, the amount of radiation entering the top of the atmosphere is similar in both hemispheres, but the amount transmitted through the atmosphere and reaching the surface can differ, for example, depending on prevailing solar angles in different seasons. Outside of the tropics, a disproportionate amount of the annual radiation at the surface is accumulated during the summer months, with contributions from winter months becoming progressively less important at higher latitudes. The closeness of the dates of the orbital perihelion (ca. 3 Jan.) and of the summer solstice in the southern hemisphere (ca. 21 Dec.) results in the surface of the southern hemisphere accumulating more radiation over the year. In M21, the annual variation was ignored since that calculation was limited to the USA but is included in the present study because it contributes to UV radiation exposure differences between Australia and the USA.

2.3. Stratospheric Ozone

Stratospheric O_3 data used here are based on measurements of the O_3 column by the TOMS instrument aboard the NIMBUS-7 satellite over the period 1980–1991 (McPeters et al., 1996). In this period, ODS emissions were higher than at any time before or after, increasing EESC sharply from ca. 1,200 to 1,700 ppt. During the same time, reductions in O_3 became evident at middle and high latitudes. Thus, the 1980s provided a unique opportunity for empirical estimation of the response of O_3 to EESC, based on global satellite observations. We use here two sets of O_3 values, both functions of latitude and month: the initial 1980 (intercept) values, and the trend (slope) over 1980–1990.

It is important to note that the AHEF uses the O_3 data on a monthly basis, not as coarser annual averages. This temporal resolution is particularly important to compute accurate annual UV exposures, with summer O_3 trends contributing more than winter trends. The evolution of O_3 calculated for the A1 scenario is discussed in Section 3.6.

2.4. Baseline Cases and Deaths

The AHEF defines "baseline" cases (incidence) and deaths (mortality) as what would be expected to occur if stratospheric O_3 concentrations remained fixed at 1980 levels. The derivation of baseline rates for the U.S. population is discussed in M21. The derivation of baseline rates for each UV-related health effect for the Australian population is outlined in Table 1 and discussed in more detail below. In cases where the available data do not allow calculation of a 1980 baseline, we use the closest available year.

Melanoma case and death rates were derived by applying the national 5-year age-group profiles (AIHW, 2025a) to the sex-specific total for each state (AIHW, 2025b), giving baseline case and death rates by state, sex, and 5-year age group. *Keratinocyte cancer case* rates were derived as the sex-specific sum of basal and squamous cell carcinoma (BCC and SCC, respectively) in each of 3 latitude bands for a 1985 (Staples et al., 1998) baseline and distributed by age in proportion to the 2002 10-year age group incidence data (Staples et al., 2006). *Keratinocyte cancer mortality* data are used as reported on a national basis, segregated by sex and 5-year age group (AIHW, 2025b). *Cataract rates* were derived by distributing the national total hospitalization rates for people aged 40 (AIHW, 2015, 2017) in proportion to the 10-year age group case distribution from a regional study

Table 1
Australian Baseline Cases and Mortality Data

Malady	Baseline year(s)[a]	Data distribution		Source information
		Source	As used	
Melanoma Incidence	1982–1985[b]	State all-age totals; national 5-year age group totals	By state and 5-year age group	AIHW (2018, 2025a)
Melanoma Mortality	1976–1980	State all-age totals, nationally by 5-year age group	By state and 5-year age group	AIHW (2018, 2025b)
Keratinocyte Cancer Incidence	1985	Age-standardized rates by latitude band (1985);[c] national 10-year age group rates (2002)	By latitude band and 10-year age group	Staples et al. (1998, 2006)
Keratinocyte Cancer Mortality	1976–1980	National by 5-year age group	National by 5-year age group	AIHW (2025b)
Cataract (hospitalization) Incidence	2013–2015	National totals; rates by 10-year age group (regional study, mid-1990s)	National by 10-year age group	AIHW (2015, 2017), Panchapakesan et al. (2003)

Note. AIHW, Australian Institute of Health and Welfare. [a]Several years of data (if available) are averaged into the baseline value to smooth out noise. [b]Available data begin in 1982. [c]Latitude bands are: <29°S, 29–37°S, >37°S.

(Panchapakesan et al., 2003). Cataract hospitalization rates have increased significantly in recent years, likely in response to healthcare improvements (Keeffe & Taylor, 1996). Therefore, using recent hospitalization data is more meaningful than estimating 1980 baseline rates for this malady.

2.5. Population Data

Historical and projected population data for Australia are taken from the Australian Bureau of Statistics (ABS, 2023a, 2023b). The data are reported by Statistical Area (SA) annually from 1980 to 2018. Annual population projections are given by state or territory from 2018 to 2066 and are subdivided by sex and 5-year age group between 0 and 84 with one combined group for ages of 85 and above. We distributed these projections at the SA4 level (the largest sub-state regions) in proportion to the 2018 reported data.

2.6. Skin Types

Light skin generally shows greater response to UV radiation than does dark skin (Brenner & Hearing, 2008; Trakatelli et al., 2017). To assess the sensitivity of the malady results to skin type variations in the study populations, we defined upper- and lower-response limit cases, using the approach of the Fitzpatrick skin phototype classification, which is widely used to assess risk factors such as UV exposure for skin cancers (Brenner & Hearing, 2008). Worldwide, majority-light-skinned populations are given a I or II categorization, while populations with skin of color often have Fitzpatrick skin phototypes III to VI (Torres et al., 2017).

The Australian health and population data do not include a skin type category, so we categorized the state-by-state population data into a Fitzpatrick-like scale of I to VI according to self-reported ancestry (ABS, 2011, 2016) using guidance from Trakatelli et al. (2017) and Torres et al. (2017). Our upper-response limit classifies the entire population (phototypes I-VI) as light-skinned. Our lower-response limit assigns skin phototypes I-II as "light" and III–VI as "dark," giving a ratio of 4:1 between the sizes of the "light-" and "dark-skinned" categories. We did not assign temporal trends since no ancestry projections are available for Australia. The U.S. baseline health and population data are already categorized (per M21) into two and three different skin types respectively, effectively "light"/"dark" or "light"/"dark"/"other." This gives a low-response limit in the USA initially like that in Australia, with the "light":"dark" ratio evolving from 4:1 to 2:1 between 2000 and 2060, while the U.S. upper response limit ratios evolve from 7:1 to 6:1 over the same period. The calculations presented in this paper use the mean of the upper- and lower-response limits for both countries.

2.6.1. Dose-Response Relations and Biological Amplification Factors

The dose-response relationship in the AHEF model is parameterized with a power dependence,

$$\text{Response} \propto (\text{Dose})^{\text{BAF}} \quad (1)$$

here, the response is the baseline incidence of a given malady, the dose is the cumulative UV radiation received, and the Biological Amplification Factor (BAF) is a dimensionless malady-specific exponent (normalized sensitivity coefficient), the percent increase in response for a 1% increase in UV dose. The BAFs used in the AHEF were derived from U.S. health data (Pitcher & Longstreth, 1991; West et al., 2005) or from studies on hairless mice (de Gruijl & Forbes, 1995) (see Table 3 of M21). Their values range from 0.17 to 0.24 (±0.09) for cataracts (West et al., 2005), 0.50–0.58 (±0.4) for melanoma incidence and mortality (Pitcher & Longstreth, 1991), and up to 2.8 (±0.8) for SCC incidence (de Gruijl & Forbes, 1995). The magnitude of the error estimates should be noted. For melanoma in particular, the original reported error included only the standard error of the fit and was revised from ±0.02 to ±0.4 by van Dijk et al. (2013). Such large BAF errors have a dominant role in the overall uncertainty of the AHEF calculation chain. We use the same BAF values for both the USA and Australia.

2.7. Trend Analysis

Analyses of modeled malady time trends were carried out using Poisson regression using SPSS V. 23 (Ely et al., 1997) to estimate the annual percentage change (APC) in the rates over the entire study period. Model results are deterministic and do not contain scatter, hence 95% confidence intervals are not reported.

2.8. ARPANSA UV Radiation Measurement Network

The Australian Radiation Protection and Nuclear Safety Agency (ARPANSA) maintains a network of UV sensors to monitor solar radiation in numerous cities and population centers across Australia at latitudes from 12°S to 43°S. Originally employing Robertson-Berger type broadband radiometers (UV Biometer model 501, Solar Light Company, Philadelphia, USA), since 2017 the network has used SiC photodiode UV sensors (Cosine UV Index Sensor, sglux GmbH, Berlin, Germany) to record the erythemally weighted UV irradiance values every minute (Henderson et al., 2018). All UV sensors are calibrated against a spectroradiometer (model DTMc300, Bentham Instruments Limited, Reading, UK) at the ARPANSA laboratory in Melbourne prior to deployment at remote monitoring sites. UV sensor performance was evaluated monthly by comparison against model calculations on clear sky days. The Robertson-Berger detectors were typically changed every 2 years, while the SiC photodiode UV sensors were far more stable and were not changed during this study. The mean annual UV dose was determined for 12 sites: Adelaide, Brisbane, Darwin, Perth and Sydney over the years 1996–2019; Newcastle and Townsville 1997–2019; Kingston 2007–2019; Canberra 2010–2019; Cairns 1996–2003; Melbourne 1993–2019; Alice Springs 1996–2000 and 2011–2019.

3. Results and Discussion

3.1. Decadal Trends of UV-Induced Health Effects

The AHEF model predicts malady incidence rates that increase with time due to aging in the Australian and U.S. populations: these same incidence rates show little or no trend when age-standardized (Figure 1 and Table 2). A small incidence rate decrease, of −0.1% annually, is noted for the USA (Table 2) and is attributed to the future demographic shifts discussed in Section 2.6. For Australia the overall long-term trends are negligible, although a slight increase is noted during the current several decades, due at least in part to the depletion of stratospheric O_3 (see Section 3.6). A prominent feature of Figure 1 is that the standardized melanoma incidence rates in Australia are significantly larger than those in the USA, as is also true for other UV-dependent maladies (Table 2).

3.2. Interhemispheric Differences for Clear Skies

Solar UV irradiance differs at equivalent SH and NH latitudes due to factors such as seasonal ESD variation and interhemispheric differences in stratospheric O_3 (as discussed earlier and modeled in the AHEF), as well as more local factors such as clouds, aerosols, and surface reflections that are currently not included in the model.

The calculated clear sky differences are shown in Figure 2. Irradiances in both hemispheres are highest near the equator and decrease toward the poles. There is an interhemispheric difference, increasing slightly with latitude,

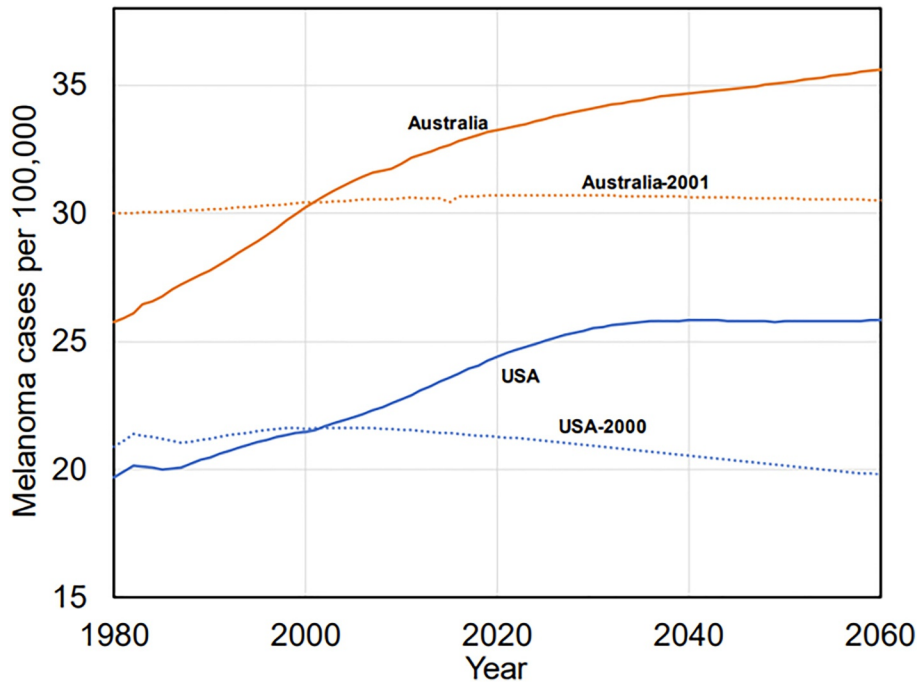

Figure 1. Melanoma incidence rates (per 100,000) for Australia (orange) and USA (blue), projected with the AHEF model from a 1980 baseline. Solid lines represent model-projected raw incidence rates that reflect the underlying population aging projections (ABS, 2023b; U.S. Census Bureau, 2019); dotted lines represent model-projected age-standardized incidence rates, incorporating the Australia-2001 (ABS, 2023a) and USA-2000 (Anderson & Rosenberg, 1998a, 1998b) standardizations.

with Australian locations subject to 5%–9% more annual UV than U.S. locations at the same absolute latitude. To isolate the orbital contributions, we repeated the UV calculation assuming a constant ESD. The remaining interhemispheric difference is then entirely attributable to O_3 column differences (open circles in Figure 2). At 35°

Table 2
Annual New Cases/Deaths (Upper Lines) and Age-Standardized Incidence Rates (per 100,000) (Lower Lines) for Australia and USA, Projected With the AHEF Model for Selected Years; and Incidence Rate Trends Projected for 1980–2020 and 1980–2060

	Australia					USA				
	1980	2020	1980–2020 trends (APC)	2060	1980–2060 trends (APC)	1980	2020	1980–2020 trends (APC)	2060	1980–2060 trends (APC)
Melanoma cases	3,790 30.0	8,590 30.7	– 0.1	14,400 30.5	– 0.0	46,900 20.9	80,500 21.3	– 0.0	104,000 19.8	– −0.1
Melanoma deaths	557 4.58	1,370 4.7	– 0.1	2,410 4.7	– 0.0	5,120 2.4	9,790 2.5	– 0.1	13,900 2.4	– −0.1
KC cases	153,000 1,302	412,000 1,370	– 0.1	740,000 1,360	– 0.0	482,000 222	912,000 226	– 0.1	1,290,000 210	– −0.1
BCC cases	121,000 1,022	320,000 1,070	N/C	572,000 1,070	N/C	387,000 178	720,000 179	N/C	1,000,000 126	N/C
SCC cases	32,600 280	90,300 298	N/C	165,000 297	N/C	94,700 43.6	192,000 46.5	N/C	291,000 43.7	N/C
KC deaths	184 1.7	600 1.9	– 0.2	1,284 1.9	– 0.1	1,880 0.90	3,790 0.92	– 0.1	6,860 0.91	– 0.0
Cataract cases	94,000 876	285,000 879	– 0.0	579,000 879	– 0.0	572,000 252	1,080,000 252	– 0.0	1,670,000 252	– 0.0

Note. Each cell contains total counts (upper row) and age-standardized rates per 100,000 (Australia-2001 or USA-2000, lower row). N/C, Not calculated; KC, Keratinocyte Carcinoma; BCC, Basal Cell Carcinoma; SCC, Squamous Cell Carcinoma; APC, Annual Percentage Change.

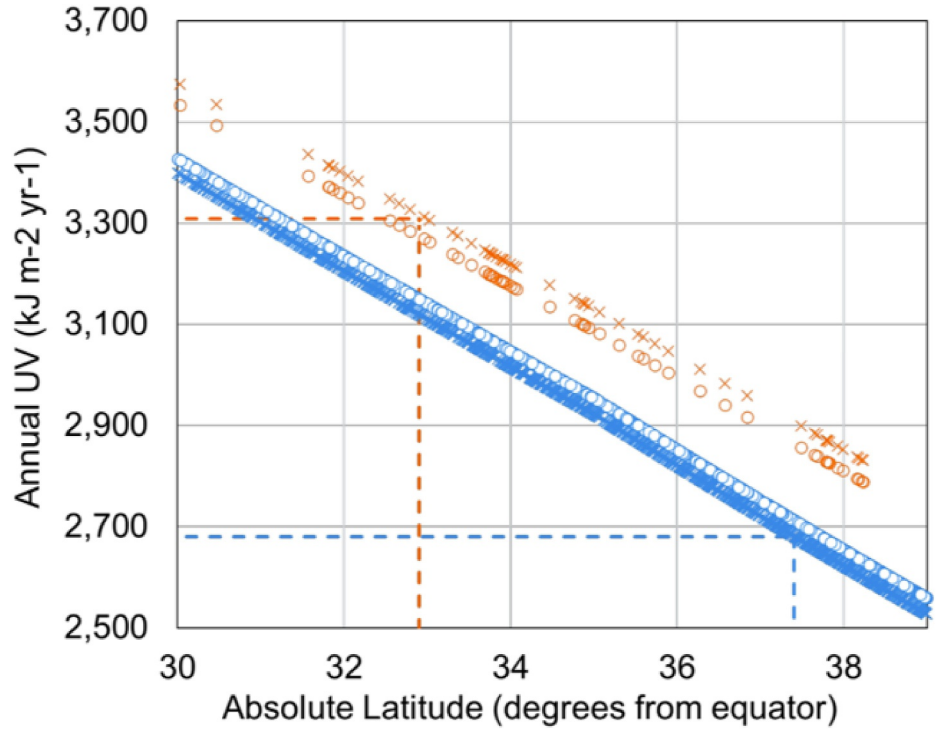

Figure 2. Annual clear-sky UV exposure for the USA and Australia (kJ m^{-2} $year^{-1}$) in the year 2000, estimated by the AHEF model using the WMO A1 ODS emissions scenario (WMO, 2018) and a 1980 O_3 baseline. Symbols are plotted at the latitudes of each county (for the USA) or Statistical Area Level 4 (SA4) (for Australia): orange, Australia; blue, USA; crosses, full calculation; open circles, calculation excluding the influence of ESD differences (i.e., including ozone difference only). Dashed lines show the annual UV radiation exposure at the population-centroid latitudes of each country.

(roughly the midpoint of the U.S. and Australian population distributions), differences in ESD account for UV irradiance increases in Australia relative to the USA of 76 kJ m^{-2} $year^{-1}$ (2.6% of the annual mean), while O_3 differences account for 127 kJ m^{-2} $year^{-1}$ (ca. 4.1%). The small latitudinal increase of the ESD effect is due to the more pronounced winter-summer difference with increasing distance from the equator.

3.3. Differences in Population Distributions

In addition to the ca. 5%–9% interhemispheric difference in sea-level UV irradiance at equivalent latitudes, the two countries experience different population-weighted UV exposure rates because of differences in their populations' latitudinal distributions (Figure 3). The population centroids for the USA and Australia are located at 37.4°N and 32.9°S, respectively, and this shift of 4.5° toward the equator translates to a ca. 13% increase in annual UV radiation (Figure 2). The equatorward displacement of the Australia population relative to the U.S. population is, thus, the dominant contributor to the Australia-USA UV difference. When the interhemispheric UV differences and the population distribution factor are combined, we find a population-weighted UV exposure value for Australia 1.24 times larger than that of the USA: 3,300 versus 2,670 kJ m^{-2} $year^{-1}$ for the year 2000 in Australia and the USA respectively.

If all other factors remain the same, Equation 1 predicts that increasing UV doses by a factor of 1.24 will increase cataract by factors of 1.04 (BAF = 0.17) and SCC by 1.79 (BAF = 2.7), factors which are far less than the actual incidence ratios between the countries (see Table 3). Use of Equation 1 with national population-weighted exposures should be done with some caution given its nonlinear nature. In the next section, we describe more detailed computations (at the statistical area level for Australia and county level for the USA), which indicate similar results and do not change this conclusion.

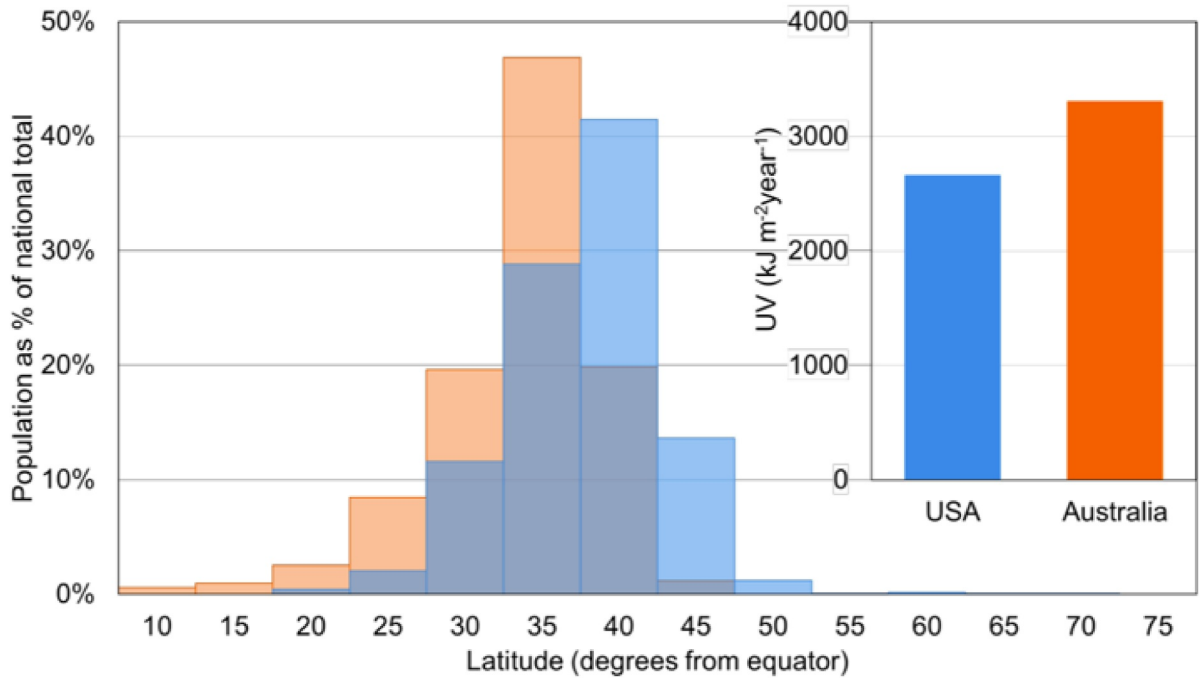

Figure 3. Year 2000 population distribution by latitude for Australia (orange) and USA (blue), expressed as percentages of total national population. Inset: Year 2000 population-weighted UV exposure (kJ m^{-2} $year^{-1}$), assessed as the sum over all Statistical Area Level 4 (SA4) regions (Australia) or counties (USA) of the local products of population and UV exposure, divided by national population.

3.4. Evaluation of Nonlinear Dose-Responses at the National Level

In the previous section, the Australia/USA ratio of population-weighted annual UV doses was estimated to be about 1.24 under clear skies. This simple metric is directly useful for linear dose-response relations, such as Equation 1 with BAF = 1. The question arises whether this simple ratio can also be used with the nonlinear dose-response functions used here, which have BAFs ranging from a low of 0.2 for cataract to a high of 2.8 for SCC incidence (see Section 2). Locations with higher UV levels (e.g., closer to the equator) may contribute disproportionally more to the national totals if BAF > 1, and disproportionally less if BAF < 1.

In the full AHEF calculation, the national-level response is evaluated by summing local responses, so that for each country

Table 3
Estimated Contributions of UV Radiation to Difference in Skin Cancer and Cataract Incidence Between Australia and the USA

Malady	BAF[a]	Expected ratio[b] from dose-response, Australia/USA	Actual ratio[c] Australia/USA
Melanoma incidence	0.54 ± 0.4	1.03–1.22	1.36
Melanoma mortality	0.54 ± 0.4	1.03–1.22	1.78
Keratinocyte mortality	0.59 ± 0.4	1.04–1.23	2.03
BCC incidence	1.40 ± 0.5	1.21–1.50	5.66
SCC incidence	2.6 ± 0.7	1.50–2.03	6.00
Cataract incidence	0.21 ± 0.1	1.02–1.07	3.05

Note. CC, Basal Cell Carcinoma; SCC, Squamous Cell Carcinoma; BAF, Biological Amplification Factor; AHEF, Atmospheric Health Effects Frameworka Biological Amplification Factors (BAFs) from M21. [a]Biological Amplification Factors (BAFs) from M21. [b]Ratios estimated as $(1.24)^{BAF}$, where the factor 1.24 is the ratio of population-weighted annual UV radiation. Ranges are estimated from BAF error bounds. [c]Ratio of actual baseline incidences, age standardized, evaluated in the year 2020 within the AHEF.

$$\text{National Response} = \frac{\sum_i P_i (UV_i)^{\text{BAF}}}{\sum_i P_i} \quad (2)$$

where P_i and UV_i are the local population and annual UV dose, respectively, and the sum over locations is denoted by the index i (ca. 3,000 counties for the USA and ca. 100 statistical areas for Australia). We compared the ratio of national responses for the two countries based on these detailed summations for different BAFs, to the ratio obtained by simply raising the (linear) UV ratio, 1.24, to the relevant BAF power.

$$\text{Australia/USA ratio of response} \approx (1.24)^{\text{BAF}} \quad (3)$$

Remarkably, this approximation gave nearly identical results to those of the full calculation, with deviations less than a few percent. For example, a detailed calculation with BAF = 3.0 gave an Australia/USA ratio of 1.86, which is only slightly overestimated by $(1.24)^3 \approx 1.91$, while for BAF = 0.2 the detailed value of 1.046 compares well with the approximate $(1.24)^{0.2} \approx 1.044$. Therefore, we suggest that this simple formulation can be used for rapid and intuitive estimates of the Australia/USA ratios expected with nonlinear dose-response functions having different BAF values.

Table 3 shows the Australia/USA ratios expected on the basis of Equation 3, using the clear sky annual UV ratio (1.24) with different BAF values. As noted earlier, the uncertainties in BAFs are quite large, and their inclusion leads to a wide range of expected Australia/USA ratios. The last column of the table shows the actual Australia/USA incidence ratios (as estimated with the AHEF for the year 2020; see also Table 3). Without exception, the actual ratios are larger than those expected from the nonlinear response to UV differences alone. Thus, it appears that ambient UV differences fall well short of explaining the higher incidence of UV-related maladies in Australia compared to the USA.

3.5. Effects of Clouds and Aerosols

Neither clouds nor aerosols are currently included in the AHEF, since the model focuses on attribution of surface UV changes to stratospheric O_3. Given the multiplicative nature of stratospheric and tropospheric transmission, this approach is suitable for estimating the relative changes (e.g., percent) in surface UV due to changing stratospheric O_3. The effects of long-term changes in clouds or aerosols can be regarded as mostly superimposable onto these, and do not change the relative sensitivity of UV radiation to stratospheric ozone (Anton et al., 2011). It is nevertheless interesting to consider how clouds and aerosols may affect surface UV irradiances differently in the USA and Australia.

Clouds usually reduce the amount of UV radiation reaching the surface, although somewhat less at UV than visible wavelengths, because Rayleigh scattering by air molecules already provides a diffuse background at the shorter wavelengths (Blumthaler et al., 1994). If large amounts of UV-absorbing gases (e.g., tropospheric O_3) are present together with optically thick clouds, enhanced absorption can occur due to long path lengths of scattered photons (Mayer et al., 1998). Occasionally, partial cloud cover can increase ground-level UV radiation above clear sky values, but these enhancements are usually limited in space and time (Crawford et al., 2003; Nack & Green, 1974).

Satellite-based observations confirm the strong variability of cloud cover at different temporal and spatial scales but can nevertheless be used to estimate climatological reductions in UV radiation reaching the surface. A climatology for the years 1979–2000 (Lee-Taylor et al., 2010; Lee-Taylor & Madronich, 2007) showed cloud-influenced transmission factors for annual erythemal UV radiation of ca. 0.7–0.8 for the contiguous USA, and 0.8–0.9 for the population-dense coastal Australia (see Figure 4). Similar UV transmission factors for clouds over Australia were found by Udelhofen et al. (1999) for the years 1979–1991, and by Lemus-Deschamps et al. (2004) for 1997–2001.

Aerosols, or suspended particulate matter (PM), have long been recognized to affect surface UV irradiances. Liu et al. (1991) calculated regional reductions of 5%–18% due to sulfate aerosols, relative to preindustrial (aerosol-free) values. Wenny et al. (1998) measured reductions of 17%–22% in rural North Carolina (USA), while Reuder and Schwander (1999) estimated aerosol-driven reductions in Europe ranging from 20% to as much as 40% in particularly polluted regions. Seckmeyer et al. (2008) found that surface UV irradiances in Europe were generally

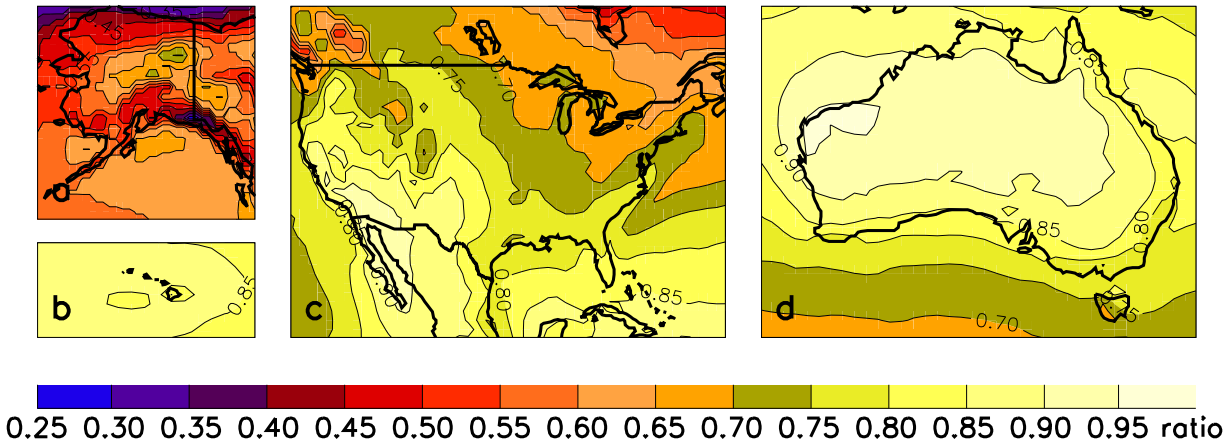

Figure 4. Climatological cloud transmission factors (1.00 = no cloud) for annual mean irradiances at erythemally weighted UV wavelengths, observed from satellite-based instruments during 1979–2000 (adapted from Lee-Taylor and Madronich (2007) and Lee-Taylor et al. (2010)).

lower than those measured at comparable latitudes in New Zealand, due mostly to differences in total O_3 and aerosol loading. In polluted megacities the UV reductions often reach or exceed 30%–40%, for example, in Santiago, Chile (Cabrera et al., 2012) and Mexico City (Ipiña et al., 2021) and have been shown to be caused mostly by aerosols, with smaller contributions from ground-level O_3 and the dioxides of nitrogen and sulfur.

Unfortunately, satellite-based instruments are currently limited in their ability to quantify urban aerosols. Gao et al. (2010) compared satellite-based estimates of erythemal UV radiation to values measured over 2000–2005 at eight non-urban sites of the US Department of Agriculture (USDA) UV-B monitoring network and found systematic overestimation ranging from 2% to 16%. Satellite-based calculations by Lee-Taylor et al. (2010) showed good agreement with ground-based observations at pristine Canadian locations, but overestimation by 10%–30% for larger cities in Canada, the USA, Japan, and Taiwan for which ground-based observations were available. Zhang et al. (2019) compared erythemal UV irradiances estimated from the satellite-borne Ozone Mapping Instrument to 31 stations of the USDA UV-B monitoring network over 2005–2017, and found a systematic overestimation of about 7%, likely due to incomplete correction for absorbing aerosols.

Aerosol optical depths have decreased substantially in the past few decades in many parts of the world (including the USA) due to air quality regulations (Carino et al., 2024; Ipiña et al., 2021; Parrish et al., 2011). For Australia, long-term (1959–2021) visibility data suggests that these reductions occurred mostly before the year 2000, with small or insignificant trends since (Hao et al., 2024). In recent decades, measurements of aerosol optical depth from ground and satellite platforms show a mix of positive and negative trends over Australia, with increases more common (Ma et al., 2025; Mitchell et al., 2017; Nuñez et al., 2022; Shaylor et al., 2022; Yang et al., 2021). Air quality data from several major Australian cities also show minor or insignificant improvements in recent aerosol burdens (Barnett, 2012; de Jesus et al., 2020). However, the increasing frequency of wildfires could be offsetting some of these trends in both the USA (Carino et al., 2024) and Australia (Kalashnikova et al., 2007; Nuñez et al., 2022; Ulpiani et al., 2020). All these changes occur during the lifespan of the populations considered in our study, further complicating the estimation of cumulative exposure.

Figure 5 illustrates the long-term effects of clouds and aerosols on the comparison between observed UV radiation at ground level in several Australian cities, and those from satellite-based instruments estimated by Lee-Taylor et al. (2010). Reductions due to clouds are seen as the difference between open and filled points, consistent with the 10%–20% reductions derived from satellite observations seen in Figure 4. The remaining differences (between the filled points and the 1:1 line) may be due to the influence of urban pollutants that are not resolved by the much larger satellite footprint (ca. 1° × 1° latitude-longitude), but may also be related to uncertainties in instrument calibrations and radiative transfer modeling.

In summary, clouds and aerosols both tend to reduce surface UV radiation. Based on satellite climatology (Figure 4) cloud-induced UV reductions of 20%–30% are common for the contiguous USA while 10%–20% reductions are more typical for coastal Australia. The effects of aerosols are more difficult to generalize as they

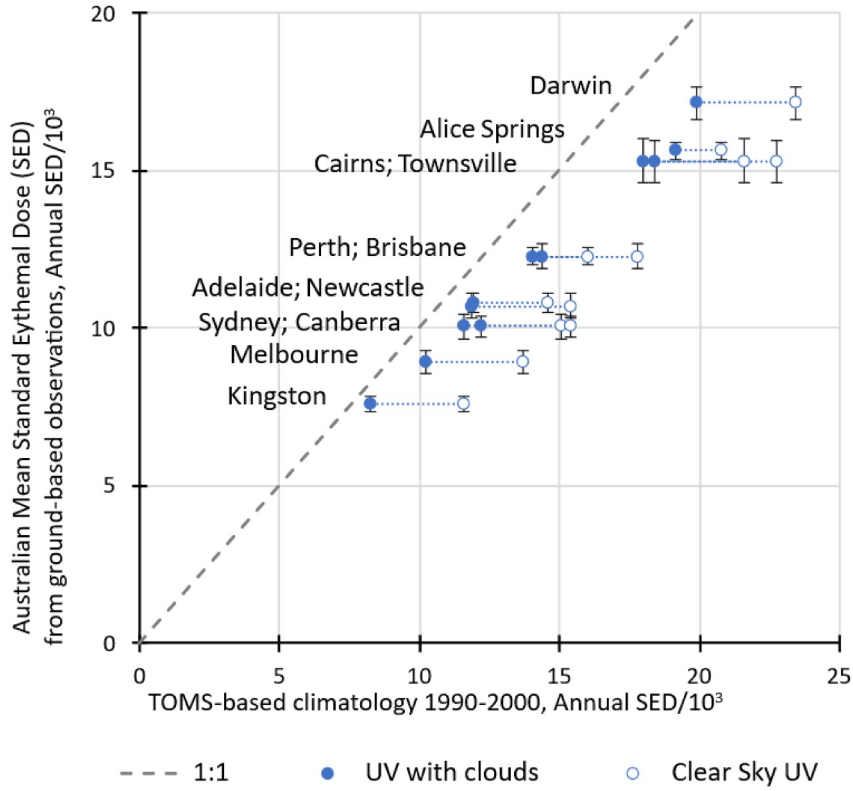

Figure 5. Comparison of annual erythemal irradiance computed from satellite-based observations of ozone and clouds (TOMS) from Lee-Taylor et al. (2010) with ground-based observations from the ARPANSA network (updated from Henderson et al. (2018)). Open circles indicate cloud-free estimates; filled circles include the effects of clouds (but not aerosols); fine dotted lines connect estimate pairs at the same location. Error bars indicate one standard deviation of the ground-based measurements. Measurement dates vary by location and are listed in Section 2.8.

depend on local conditions and long-term trends in air quality. Based on comparisons of ground-based observations with satellite-derived estimates for Australia (Figure 5) and other locations (Lee-Taylor et al., 2010), we estimate that aerosols could reduce surface UV radiation by 10%–30% in each country, and could add an additional ∼10% uncertainty to the estimated UV ratio between the two countries.

3.6. Response to Ozone Trends (A1 Scenario)

Atmospheric O_3 controls the amount of UV radiation reaching the surface and the consequent health impacts. The evolution of O_3 under the A1 emissions scenario is shown in Figure 6 for different latitude bands. For simplicity, annual averages are shown in the figure, but (as already noted) the AHEF calculations are performed with monthly resolution. Starting in 1980, O_3 decreases at all latitudes considered, reaching a minimum in ca. 1996, and recovering back to 1980 values by the middle of the 21st century. Compared to the NH, the SH has lower climatological values of O_3 and experienced stronger depletion from the increase in ODS concentrations during the 1980s. It should be recalled that these are not actual projections of O_3 levels, but only the changes in O_3 that can be attributed to ODS changes. Other factors, natural and anthropogenic, can exert multiple influences on O_3. Nevertheless, the O_3 evolutions shown in Figure 6 are broadly consistent with those recently assessed (e.g., WMO, 2022) from satellite-based and ground-based observations over the historical time period 1979–2020, for example, see Figure 3.6 of WMO (2022).

The increase in annual UV radiation due to ODS-induced stratospheric O_3 depletion as estimated by the AHEF is shown in Figure 7, for 35° latitudes. O_3 depletion and UV increases peaked at 3%–4% (for annual mean O_3, see Figure 6) and 4%–5% (for UV) in the early 1990s, after which they began to decrease in response to decreases in ODS-derived EESC concentrations. Return to pre-1980 O_3 and UV levels is expected by the mid-2040s, following the A1 ODS emissions scenario, as discussed by M21 and the latest SAP assessments

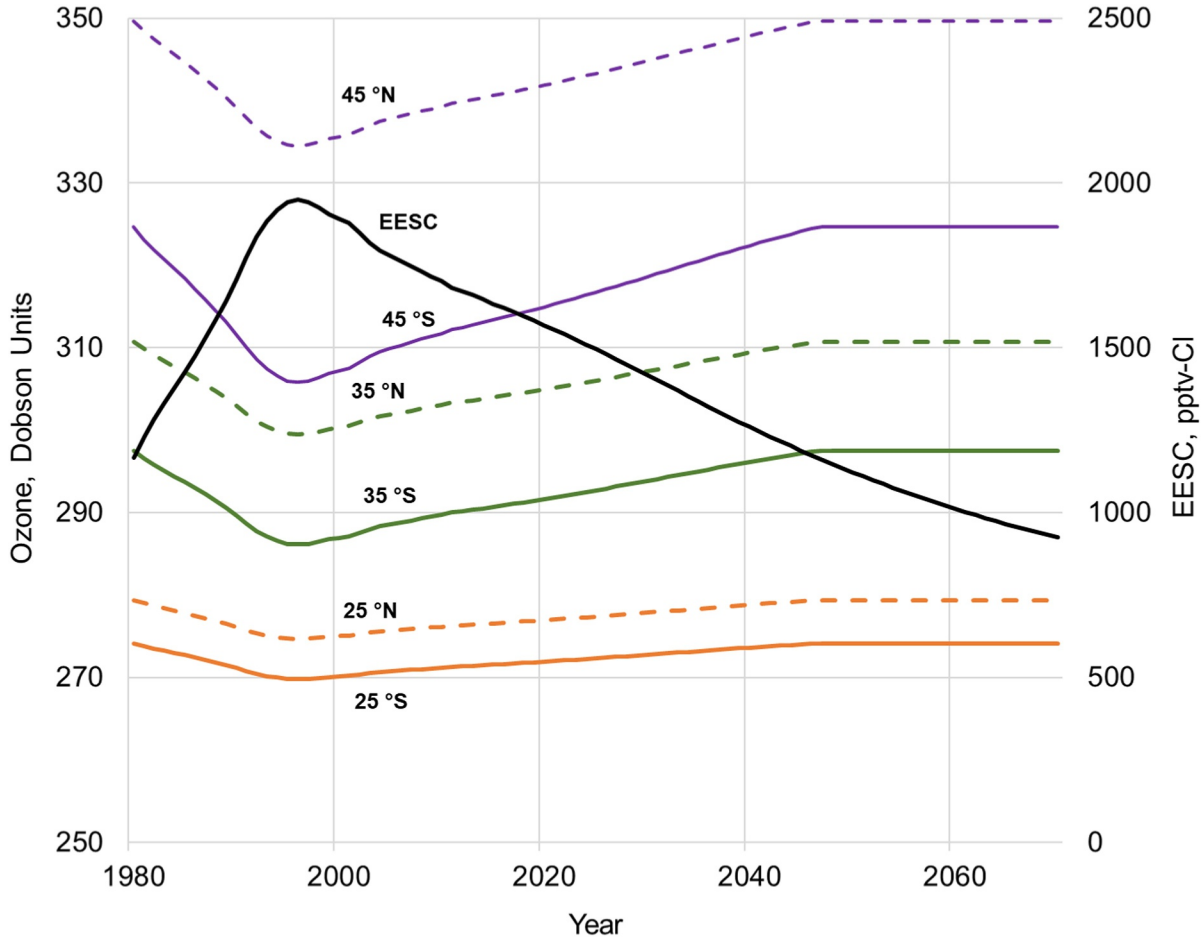

Figure 6. EESC and O_3 column corresponding to the WMO-A1 ODS emissions scenario, for the period 1980–2060. Black solid line, EESC (pptv Cl, right axis); colored lines, estimated O3 column (DU, left axis), annotations show latitudes of O_3 projections.

(WMO, 2018, 2022). Figure 7 also shows the relative increase in skin cancer and cataract cases associated with O_3 depletion. Predicted peak increments range from 0.4% for cataract, to 4.7% for SCC, in proportion to their respective BAFs. The relative values are generally smaller than those for UV radiation, because the BAF values for all maladies shown here except BCC and SCC incidence are smaller than unity, and the impacts are spread out over time. The apparent lag time (relative to the excess UV radiation) is a consequence of the assumption that age-specific incidence is proportional to cumulative lifetime exposure, so that excess UV exposure in early life continues to enhance risk for the remainder of that person's life. This should not be confused with a biological induction period, often several decades long, between exposure to UV radiation (or more generally carcinogens) and manifestation of the disease (for discussion of this induction period, see M21, suppl. materials). The precise timing of the peak depends also on other factors, such as differences in migration, and ethnicity trends, captured in our study by skin type according to self-reported ancestry.

It is notable that the health impacts of O_3 depletion are quite similar in the USA and Australia. Although SH O_3 depletion is greater at comparable mid-latitudes, a larger fraction of the Australian population resides at lower latitudes where depletion is less pronounced.

The increases in skin cancer and cataract incidence rates calculated here, while of some significance, are far smaller than those expected under scenarios of unabated ODS emissions. Modeling simulations of such extreme scenarios have found several-fold increases in surface UV radiation and associated health effects (Madronich et al., 2021; McKenzie et al., 2019; Newman et al., 2009; van Dijk et al., 2013). These outcomes have been avoided by international agreements to phase out ODS production, under the Montreal Protocol and its

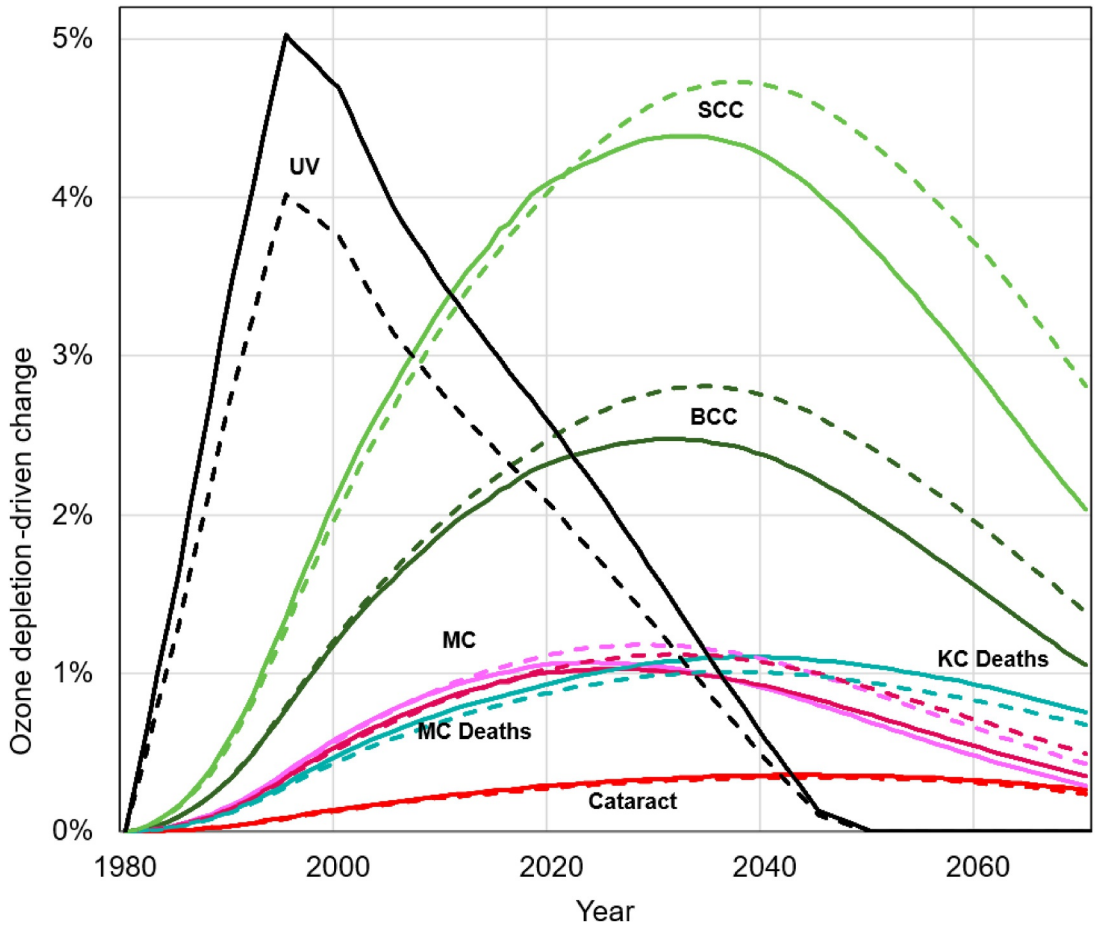

Figure 7. Increases in annual UV radiation and UV-related maladies due to ODS-derived ozone-depletion, estimated by the AHEF. Australia (solid lines), USA (dashed lines). UV exposure at 35° latitude (black). Squamous cell carcinoma (SCC) cases (light green), basal cell carcinoma (BCC) cases (dark green), melanoma cases (MC, magenta), melanoma deaths (dark red), keratinocyte carcinoma (KC) deaths (teal), cataract cases (light red). Combined KC case rate increases (not plotted) peak at 2.9% (AUS) and 3.2% (USA). Malady rates are age standardized.

amendments and adjustments, but concerns remain about future changes in stratospheric ozone from various human activities or natural events (WMO, 2022).

3.7. Other Uncertainties

Uncertainties in our health effect calculations (aside from those in the original health registry data) stem mostly from the difficulties in estimating BAFs, and to some extent the O_3-EESC correlations derived from the 1980–1991 TOMS observations. If the entire chain of calculations is carried out—from ODS emissions to total cases—estimated errors approach a factor of two (see M21). However, more accurate results can be expected if only part of the calculation chain is needed, for example, to compare the impacts of well-defined future O_3 depletion scenarios or to make comparisons on a relative basis, for example, between the USA and Australia. Uncertainties in BAFs, for example, exceeding 50% for melanoma, are the single most important factor limiting the accuracy of the overall calculation. The calculations are more sensitive to skin type classification in the USA than in Australia, where we can estimate skin type response to UV trends but not spatial gradients or evolving demographics (see Section 2.6 Skin types). The USA upper- and lower-skin type response limits contribute an uncertainty range of up to ±5% (see M21), only a small fraction of the Australia-USA differences. Projected USA skin type trends give future decreases of 1%–2% per decade in the age-standardized incidence rates, for melanoma and keratinocyte cases only (Table 3). In other words, the differences between the USA and Australia are not a result of whether and how we estimated the non-sensitive (dark skin) fraction, but rather stem from different sensitivities within the groups routinely classified as light-skinned.

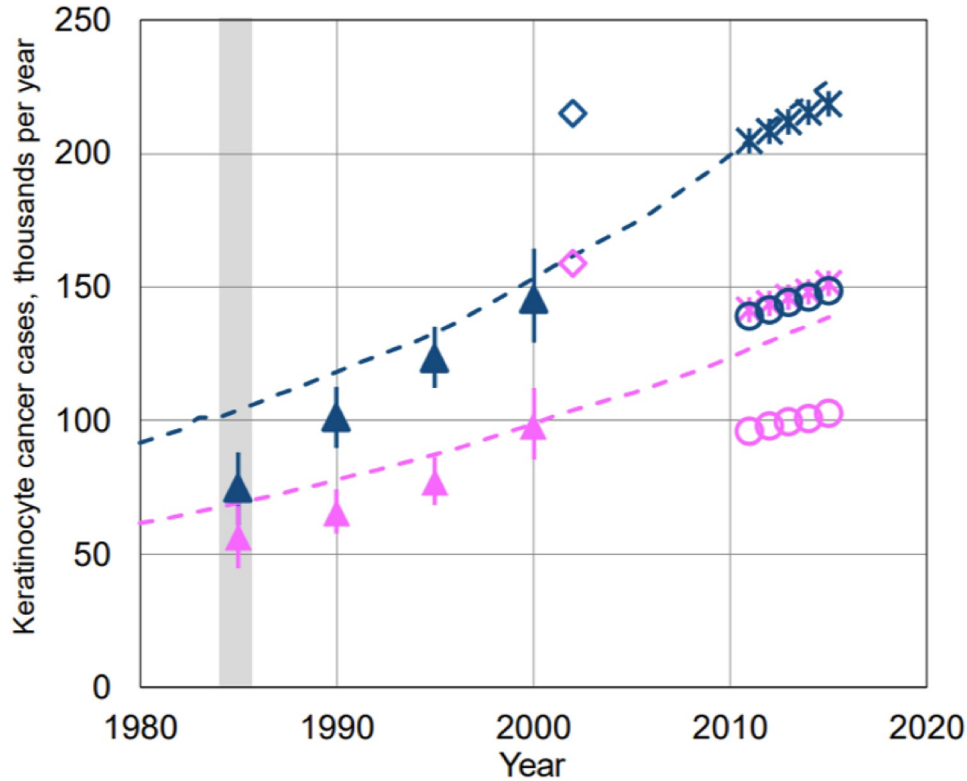

Figure 8. Model-data comparison for annual keratinocyte cancer incidence in Australia. Symbols, data; dashed lines, model calculations. Dark blue, male; pink, female. Open diamonds, "estimated AUS-wide cases" from Table 2 of Staples et al. (2006); filled triangles with solid vertical lines, product of age-standardized rates (with 95% confidence intervals) from Table 4 of Staples et al. (2006) and Australia population. Open circles, sum of basal cell carcinoma (BCC) + squamous cell carcinoma (SCC) (Pandeya et al., 2017); stars, net keratinocyte carcinoma (KC) cases (Pandeya et al. (2017). Note that the model calculations are initialized independently of the data plotted here.

3.8. Comparison to Observations

In this section we compare the model results to the observed Australian health data (comparisons for the USA are shown in Table 4 of M21). Figure 8 compares observed and modeled keratinocyte cancer (BCC + SCC) cases in Australia between 1980 and 2015. Figure 9 compares the model results with data derived from the AIHW Cancer Data in Australia database (AIHW, 2025a, 2025b). In Figure 9, the model and data should be expected to coincide within the baseline year ranges where the calculations were initialized (indicated by gray vertical shading), while agreement or divergence in later years indicates whether the model captures all factors contributing to the various malady counts.

Simulated keratinocyte incidence (Figure 8), deaths from keratinocyte cancer (Figure 9a), and melanoma deaths (Figure 9c) track the trend of the recorded cases reasonably well. In the model, the increases result mostly from population aging, with age-standardized rates being nearly constant (see Table 3 and Figure 1). The good agreement with observations supports the interpretation that aging is the main cause of the increase.

For melanoma cases (Figure 9b) the model significantly diverges from the data, underpredicting in 2020 by ~30% (for female cases) to ~50% (for male cases). Possible contributing factors to the melanoma excess (i.e., melanoma rates above AHEF-predicted values) might include changes in human behavior that increase personal UV exposure, although major behavioral changes would be inconsistent with the agreement in KC. This then suggests that different factors may be responsible, such as increased medical screening and detection for melanoma (as has been previously hypothesized for cataract incidence) (Foreman et al., 2018), or to other factors currently not identified.

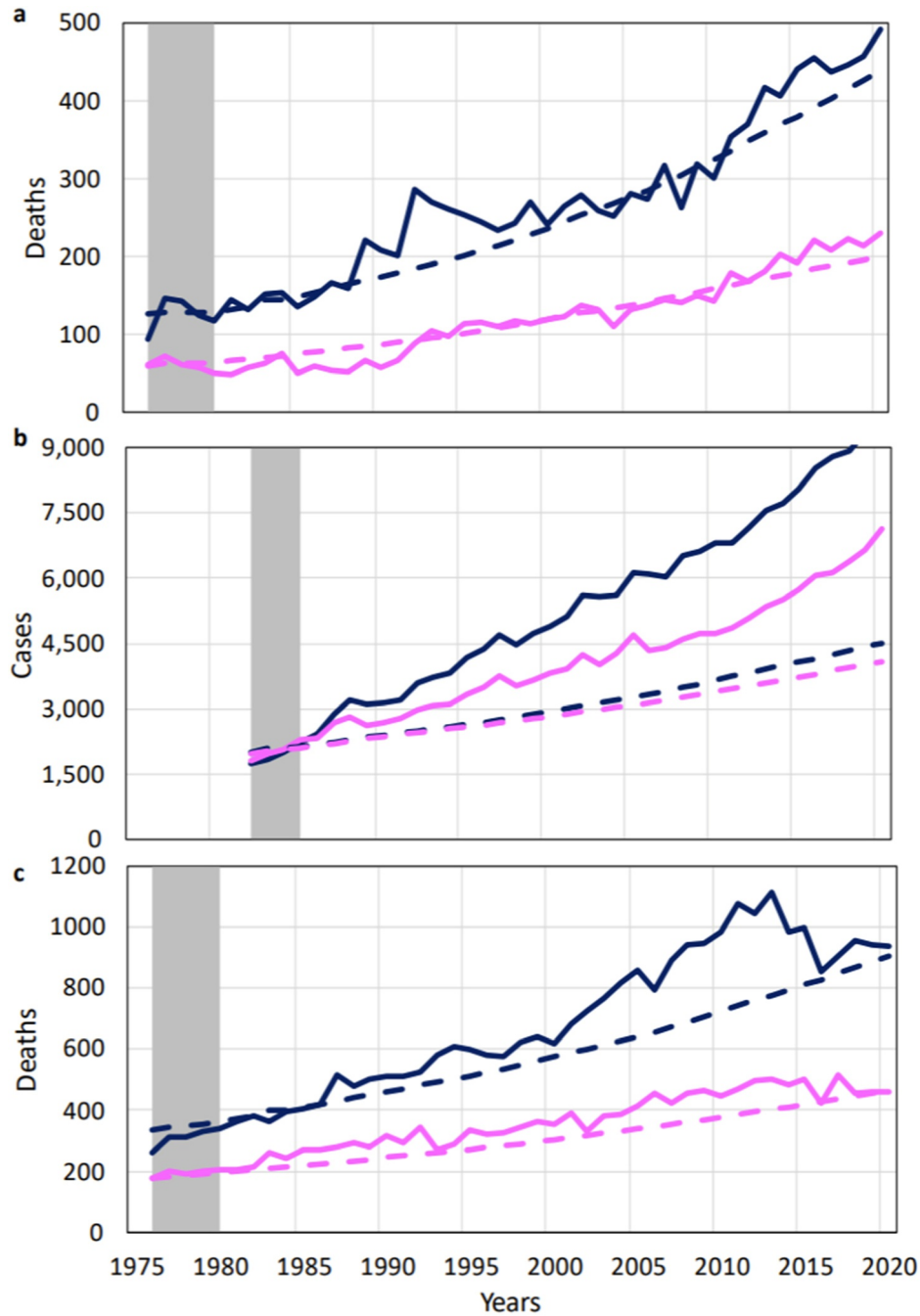

Figure 9. Comparison of modeled and reported data for Australia for (a) keratinocyte deaths, (b) melanoma cases and (c) melanoma deaths. Solid lines, data (AIHW, 2025a, 2025b); dashed lines, model. Gray bar, date range of baseline data. Dark blue, male; pink, female.

4. Conclusion

This study found that differences in population-weighted surface UV radiation between Australia and the USA can only partly explain Australia's higher incidence and mortality rates for UV-related maladies. The Australian population is potentially exposed to 24% more biologically weighted UV radiation on average than is the U.S. population because of (in approximate order of importance) closer proximity to the equator, less stratospheric O_3 at comparable latitudes, and seasonal variations in the Earth-Sun distance. Yet, the actual incidence ratios

between the two countries far exceed the predicted relationships between increased UV doses and increased maladies. Stratospheric O_3 depletion caused by ODS has increased slightly the incidence of UV-related maladies, with peak increments ranging from 0.5% for cataract to ca. 5% for SCC, and of similar size in both the USA and Australia. Thus, the contribution of stratospheric O_3 depletion to the large differences in health effects between the two countries is near-negligible.

We estimate that the effects of clouds and aerosols could each add on the order of an additional ∼10% uncertainty to the estimated UV ratio between the two countries. The effects of air pollutants (e.g., aerosols from urban emissions or wildfires) on the UV climatology are poorly known and are likely to change in the future, bringing additional uncertainty to our projected estimates.

UV-induced maladies can be viewed broadly as related to three somewhat separate factors: (a) the availability of environmental UV radiation, (b) the genetic susceptibility of individual skin types, and (c) exposure behaviors and diagnosis practices. We have addressed only the first of these, recognizing that it is currently amenable to quantification because the relevant atmospheric processes are mostly known. This study suggests that additional factors must play a substantial role in determining UV-associated incidence and mortality.

With no further projected changes in ozone-depletion-related UV radiation out to 2060, the age-standardized incidence rates for melanoma, keratinocyte cancer and cataract are also projected to remain unchanged, and the high burden of disease from these UV-related conditions is expected to persist (Garbe et al., 2024; Gordon et al., 2022; Neale et al., 2023). This supports recent assessments of the ongoing need for sun safety campaigns to educate the public on methods to reduce their risk of skin cancer by using good sun protection.

Conflict of Interest

The authors declare no conflicts of interest relevant to this study.

Availability Statement

Primary melanoma incidence data for Australia can be retrieved from AIHW (2025a) book 1a and book 7. Primary melanoma and keratinocyte mortality data for Australia have been updated by AIHW and are now publicly available only starting in 1982 (AIHW, 2025b), including melanoma mortality by age group. This study used historical data starting in 1971 that are available from AIHW on request. Primary keratinocyte cancer incidence can be accessed from Staples et al. (1998, 2006). Cataract incidence can be retrieved from (AIHW, 2015, 2017) and Panchapakesan et al. (2003). Primary population and demographic data can be obtained from (ABS, 2023a) for historical census data and (ABS, 2023b) for projections. Stratospheric ozone data and UV exposure are calculated by the AHEF model. All data generated by this study including preprocessed model input data and results are available at Lee-Taylor and Madronich (2026). The AHEF model (U.S. EPA, 2020) supporting this research is developed and maintained by EPA. AHEF is restricted EPA software and unavailable to the public or research community. General information on AHEF, including reports detailing the model, are available at https://www.epa.gov/ozone-layer-protection/atmospheric-and-health-effects-framework-model-estimating-ultraviolet.

Acknowledgments
The authors acknowledge with gratitude the cooperation and support of the Department of Climate Change, Energy, the Environment and Water (DCCEEW) Australia and the United States National Oceanic and Atmospheric Administration (NOAA). The authors would also like to thank Helena Caswell (ICF), who provided early support for processing baseline incidence and mortality data. The AHEF model is a proprietary model owned by EPA. Although the information described in this article has been funded wholly or in part by the EPA under contract 68-HER-H19-D0029 to ICF, it does not necessarily reflect the views of the Agency, and no official endorsement should be inferred.

References

ABS. (2011). National, state and territory population [Dataset]. *Australian Bureau of Statistics*. Retrieved from https://www.abs.gov.au/statistics/people/population/national-state-and-territory-population

ABS. (2016). National, state and territory population [Dataset]. *Australian Bureau of Statistics*. Retrieved from https://www.abs.gov.au/statistics/people/population/national-state-and-territory-population

ABS. (2023a). National, state and territory population [Dataset]. *Australian Bureau of Statistics*. Retrieved from https://www.abs.gov.au/statistics/people/population/national-state-and-territory-population

ABS. (2023b). Population projections Australia [Dataset]. *Australian Bureau of Statistics*. Retrieved from https://www.abs.gov.au/statistics/people/population/population-projections-australia/latest-release

AIHW. (2015). Chapter 3.2—Cataract surgery 40 years and over [Dataset]. *Australian Institute of Health Welfare*. Retrieved from https://www.safetyandquality.gov.au/our-work/healthcare-variation/atlas-2015/atlas-2015-3-surgical-interventions

AIHW. (2017). Chapter 4.6—Cataract surgery hospitalisations 40 years and over [Dataset]. *Australian Institute of Health Welfare Canberra*. Retrieved from https://www.safetyandquality.gov.au/our-work/healthcare-variation/atlas-2015/atlas-2017-4-surgical-interventions

AIHW. (2018). Australian Cancer Incidence and Mortality (ACIM) books: Melanoma of the skin [Dataset]. *Australian Institute of Health and Welfare*. Retrieved from https://www.aihw.gov.au/reports/cancer/cancer-data-in-australia

AIHW. (2025a). Book 1a—Cancer incidence (age-standardised rates and 5-year age groups), in cancer data in Australia [Dataset]. *Australian Institute of Health Welfare*. Retrieved from https://www.aihw.gov.au/reports/cancer/cancer-data-in-australia/data

AIHW. (2025b). Book 2a—Cancer mortality [Dataset]. *Australian Institute of Health Welfare*. Retrieved from https://www.aihw.gov.au/reports/cancer/cancer-data-in-australia/data

Anderson, R. N., & Rosenberg, H. M. (1998a). *Age standardization of death rates: Impllementation of the year 2000 standard*. National Vital Statistics Reports.

Anderson, R. N., & Rosenberg, H. M. (1998b). *Report of the second workshop on age-adjustment*. National Center for Health Statistics (U.S.).

Anton, M., Serrano, A., Cancillo, M. L., Garcia, J. A., & Madronich, S. (2011). Empirical evaluation of a simple analytical formula for the ultraviolet index. *Photochemistry and Photobiology*, *87*(2), 478–482. https://doi.org/10.1111/j.1751-1097.2010.00860.x

Arnold, M., Singh, D., Laversanne, M., Vignat, J., Vaccarella, S., Meheus, F., et al. (2022). Global burden of cutaneous melanoma in 2020 and projections to 2040. *JAMA Dermatology*, *158*(5), 495–503. https://doi.org/10.1001/jamadermatol.2022.0160

Arola, A., Kazadzis, S., Lindfors, A., Krotkov, N., Kujanpää, J., Tamminen, J., et al. (2009). A new approach to correct for absorbing aerosols in OMI UV. *Geophysical Research Letters*, *36*(22). https://doi.org/10.1029/2009gl041137

Barnett, A. G. (2012). Air pollution trends in four Australian cities 1996-2011. *Air Quality and Climate Change*, *46*(4), 28–34.

Bernhard, G. H., Bais, A. F., Aucamp, P. J., Klekociuk, A. R., Liley, J. B., & McKenzie, R. L. (2023). Stratospheric ozone, UV radiation, and climate interactions. *Photochemical and Photobiological Sciences*, *22*(5), 937–989. https://doi.org/10.1007/s43630-023-00371-y

Blumthaler, M., Ambach, W., & Salzgeber, M. (1994). Effects of cloudiness on global and diffuse UV irradiance in a high-mountain area. *Theoretical and Applied Climatology*, *50*(1), 23–30. https://doi.org/10.1007/BF00864899

Brenner, M., & Hearing, V. J. (2008). The protective role of melanin against UV damage in human skin. *Photochemistry and Photobiology*, *84*(3), 539–549. https://doi.org/10.1111/j.1751-1097.2007.00226.x

Cabrera, S., Ipiña, A., Damiani, A., Cordero, R. R., & Piacentini, R. D. (2012). UV index values and trends in Santiago, Chile (33.5 S) based on ground and satellite data. *Journal of Photochemistry and Photobiology B: Biology*, *115*, 73–84. https://doi.org/10.1016/j.jphotobiol.2012.06.013

Carino, H., Walsh, S., & Shakya, K. M. (2024). Long term trend of particulate matter in Philadelphia, Pennsylvania and its association with introduction of environmental policies. *Discover Cities*, *1*(1), 7. https://doi.org/10.1007/s44327-024-00007-5

Crawford, J., Shetter, R., Lefer, B., Cantrell, C., Junkermann, W., Madronich, S., & Calvert, J. (2003). Cloud impacts on UV spectral actinic flux observed during the international Photolysis Frequency Measurement and Model Intercomparison (IPMMI). *Journal of Geophysical Research*, *108*(D16). https://doi.org/10.1029/2002jd002731

de Gruijl, F. R., & Forbes, P. D. (1995). UV-induced skin cancer in a hairless mouse model. *BioEssays*, *17*(7), 651–660. https://doi.org/10.1002/bies.950170711

de Gruijl, F. R., Sterenborg, H. J., Forbes, P. D., Davies, R. E., Cole, C., Kelfkens, G., et al. (1993). Wavelength dependence of skin cancer induction by ultraviolet irradiation of albino hairless mice. *Cancer Research*, *53*(1), 53–60.

de Jesus, A. L., Thompson, H., Knibbs, L. D., Hanigan, I., De Torres, L., Fisher, G., et al. (2020). Two decades of trends in urban particulate matter concentrations across Australia. *Environmental Research*, *190*, 110021. https://doi.org/10.1016/j.envres.2020.110021

Ely, J. W., Dawson, J. D., Lemke, J. H., & Rosenberg, J. (1997). An introduction to time-trend analysis. *Infection Control & Hospital Epidemiology*, *18*(4), 267–274. https://doi.org/10.1086/647609

Foreman, J., Xie, J., Keel, S., Taylor, H. R., & Dirani, M. (2018). Utilization of eye health-care services in Australia: The National Eye Health Survey. *Clinical and Experimental Ophthalmology*, *46*(3), 213–221. https://doi.org/10.1111/ceo.13035

Gao, Z., Gao, W., & Chang, N.-B. (2010). Comparative analyses of the ultraviolet-B flux over the continental United State based on the NASA total ozone mapping spectrometer data and USDA ground-based measurements. *Journal of Applied Remote Sensing*, *4*(1), 043547. https://doi.org/10.1117/1.3507249

Garbe, C., Forsea, A.-M., Amaral, T., Arenberger, P., Autier, P., Berwick, M., et al. (2024). Skin cancers are the most frequent cancers in fair-skinned populations, but we can prevent them. *European Journal of Cancer*, *204*, 114074. https://doi.org/10.1016/j.ejca.2024.114074

Gordon, L. G., Leung, W., Johns, R., McNoe, B., Lindsay, D., Merollini, K. M. D., et al. (2022). Estimated healthcare costs of melanoma and Keratinocyte skin cancers in Australia and Aotearoa New Zealand in 2021. *International Journal of Environmental Research and Public Health*, *19*(6), 3178. https://doi.org/10.3390/ijerph19063178

Hao, H., Wang, K., Zhao, C., Wu, G., & Li, J. (2024). Visibility-derived aerosol optical depth over global land from 1959 to 2021. *Earth System Science Data*, *16*(7), 3233–3260. https://doi.org/10.5194/essd-16-3233-2024

Henderson, S., Gies, P., & Hardman, D. (2018). Introducing a new generation of solar UVR detectors for the ARPANSA UV monitoring network. In *Paper presented at the NIWA 2018 Workshop UV radiation: Effects on Human Health and the Environment, Wellington, New Zealand*. Retrieved from https://niwa.co.nz/sites/default/files/Henderson%20UV%20Sensors.pdf

Herman, J., Cede, A., Huang, L., Ziemke, J., Torres, O., Krotkov, N., et al. (2020). Global distribution and 14-year changes in erythemal irradiance, UV atmospheric transmission, and total column ozone for 2005–2018 estimated from OMI and EPIC observations. *Atmospheric Chemistry and Physics*, *20*(14), 8351–8380. https://doi.org/10.5194/acp-20-8351-2020

Ipiña, A., López-Padilla, G., Retama, A., Piacentini, R. D., & Madronich, S. (2021). Ultraviolet radiation environment of a tropical megacity in transition: Mexico City 2000–2019. *Environmental Science and Technology*, *55*(16), 10946–10956. https://doi.org/10.1021/acs.est.0c08515

Kalashnikova, O. V., Mills, F. P., Eldering, A., & Anderson, D. (2007). Application of satellite and ground-based data to investigate the UV radiative effects of Australian aerosols. *Remote Sensing of Environment*, *107*(1–2), 65–80. https://doi.org/10.1016/j.rse.2006.07.025

Keeffe, J. E., & Taylor, H. R. (1996). Cataract surgery in Australia 1985-94. *Australian and New Zealand Journal of Ophthalmology*, *24*(4), 313–317. https://doi.org/10.1111/j.1442-9071.1996.tb01601.x

Lee-Taylor, J., & Madronich, S. (2007). *Climatology of UV-A, UV-B, and erythemal radiation at the earth's surface, 1979-2000*. NCAR Technical Note.

Lee-Taylor, J., & Madronich, S. (2026). Atmospheric health effects framework model input and modeled results data for the United States and Australia [Dataset]. *ScienceHub*. https://doi.org/10.23719/d-d51x

Lee-Taylor, J., Madronich, S., Fischer, C., & Mayer, B. (2010). A climatology of UV radiation, 1979–2000, 65S–65N. UV radiation in global climate change: Measurements, modeling and effects on ecosystems (pp. 1–20).

Lemus-Deschamps, L., Rikus, L., Grainger, S., Gies, P., Sisson, J., & Li, Z. (2004). UV index and UV dose distributions for Australia (1997–2001). *The Australian Meteorological Magazine*, *53*(4), 239–250. https://doi.org/10.1071/es04026

Liu, S., McKeen, S., & Madronich, S. (1991). Effect of anthropogenic aerosols on biologically active ultraviolet radiation. *Geophysical Research Letters*, *18*(12), 2265–2268. https://doi.org/10.1029/91gl02773

Löfgren, S. (2017). Solar ultraviolet radiation cataract. *Experimental Eye Research*, *156*, 112–116. https://doi.org/10.1016/j.exer.2016.05.026

Ma, X., Morawska, L., Zou, B., Gao, J., Deng, J., Wang, X., et al. (2025). Towards compliance with the 2021 WHO air quality guidelines: A comparative analysis of PM2.5 trends in Australia and China. *Environment International*, *198*, 109378. https://doi.org/10.1016/j.envint.2025.109378

Madronich, S. (1987). Photodissociation in the atmosphere: 1. Actinic flux and the effects of ground reflections and clouds. *Journal of Geophysical Research*, *92*(D8), 9740–9752. https://doi.org/10.1029/jd092id08p09740

Madronich, S., Lee-Taylor, J. M., Wagner, M., Kyle, J., Hu, Z., & Landolfi, R. (2021). Estimation of skin and ocular damage avoided in the United States through implementation of the Montreal protocol on substances that deplete the ozone layer. *ACS Earth and Space Chemistry*, *5*(8), 1876–1888. https://doi.org/10.1021/acsearthspacechem.1c00183

Mayer, B., Kylling, A., Madronich, S., & Seckmeyer, G. (1998). Enhanced absorption of UV radiation due to multiple scattering in clouds: Experimental evidence and theoretical explanation. *Journal of Geophysical Research*, *103*(D23), 31241–31254. https://doi.org/10.1029/98jd02676

McKenzie, R., Bernhard, G., Liley, B., Disterhoft, P., Rhodes, S., Bais, A., et al. (2019). Success of Montreal protocol demonstrated by comparing high-quality UV measurements with "World Avoided" calculations from two chemistry-climate models. *Scientific Reports*, *9*(1), 13. https://doi.org/10.1038/s41598-019-48625-z

McPeters, R. D., Hollandsworth, S. M., Flynn, L. E., Herman, J. R., & Seftor, C. J. (1996). Long-term ozone trends derived from the 16-year combined Nimbus 7/Meteor 3 TOMS Version 7 record. *Geophysical Research Letters*, *23*(25), 3699–3702. https://doi.org/10.1029/96gl03540

Michalsky, J. J. (1988). The Astronomical Almanac's algorithm for approximate solar position (1950–2050). *Solar Energy*, *40*(3), 227–235. https://doi.org/10.1016/0038-092x(88)90045-x

Mitchell, R. M., Forgan, B. W., & Campbell, S. K. (2017). The climatology of Australian aerosol. *Atmospheric Chemistry and Physics*, *17*(8), 5131–5154. https://doi.org/10.5194/acp-17-5131-2017

Nack, M., & Green, A. (1974). Influence of clouds, haze, and smog on the middle ultraviolet reaching the ground. *Applied Optics*, *13*(10), 2405–2415. https://doi.org/10.1364/ao.13.002405

Neale, R., Lucas, R., Byrne, S., Hollestein, L., Rhodes, L., Yazar, S., et al. (2023). The effects of exposure to solar radiation on human health. *Photochemical and Photobiological Sciences*, *22*(5), 1011–1047. https://doi.org/10.1007/s43630-023-00375-8

Newman, P. A., Oman, L. D., Douglass, A. R., Fleming, E. L., Frith, S. M., Hurwitz, M. M., et al. (2009). What would have happened to the ozone layer if Chlorofluorocarbons (CFCs) had not been regulated? *Atmospheric Chemistry and Physics*, *9*(6), 2113–2128. https://doi.org/10.5194/acp-9-2113-2009

Nuñez, M., Serrano, A., & Larson, N. R. (2022). A climatology of aerosol optical depths in the ultraviolet wavelengths for Hobart, Australia, as determined by a Brewer MKIII spectrophotometer. *International Journal of Climatology*, *43*(1), 632–649. https://doi.org/10.1002/joc.7802

Oriowo, O. M., Cullen, A. P., Chou, B. R., & Sivak, J. G. (2001). Action spectrum and recovery for in vitro UV-induced cataract using whole lenses. *Investigative Ophthalmology and Visual Science*, *42*(11), 2596–2602.

Panchapakesan, J., Mitchell, P., Tumuluri, K., Rochtchina, E., Foran, S., & Cumming, R. G. (2003). Five year incidence of cataract surgery: The Blue Mountains Eye Study. *British Journal of Ophthalmology*, *87*(2), 168–172. https://doi.org/10.1136/bjo.87.2.168

Pandeya, N., Olsen, C. M., & Whiteman, D. C. (2017). The incidence and multiplicity rates of keratinocyte cancers in Australia. *Medical Journal of Australia*, *207*(8), 339–343. https://doi.org/10.5694/mja17.00284

Parrish, D. D., Singh, H. B., Molina, L., & Madronich, S. (2011). Air quality progress in North American megacities: A review. *Atmospheric Environment*, *45*(39), 7015–7025. https://doi.org/10.1016/j.atmosenv.2011.09.039

Pitcher, H. M., & Longstreth, J. D. (1991). Melanoma mortality and exposure to ultraviolet radiation: An empirical relationship. *Environment International*, *17*(1), 7–21. https://doi.org/10.1016/0160-4120(91)90333-L

Reuder, J., & Schwander, H. (1999). Aerosol effects on UV radiation in nonurban regions. *Journal of Geophysical Research*, *104*(D4), 4065–4077. https://doi.org/10.1029/1998jd200072

Seckmeyer, G., Glandorf, M., Wichers, C., McKenzie, R., Henriques, D., Carvalho, F., et al. (2008). Europe's darker atmosphere in the UV-B. *Photochemical and Photobiological Sciences*, *7*(8), 925–930. https://doi.org/10.1039/b804109a

Shaylor, M., Brindley, H., & Sellar, A. (2022). An evaluation of two decades of aerosol optical depth retrievals from MODIS over Australia. *Remote Sensing*, *14*(11), 2664. https://doi.org/10.3390/rs14112664

Staples, M., Elwood, M., Burton, R. C., Williams, J. L., Marks, R., & Giles, G. G. (2006). Non-melanoma skin cancer in Australia: The 2002 national survey and trends since 1985. *Medical Journal of Australia*, *184*(1), 6–10. https://doi.org/10.5694/j.1326-5377.2006.tb00086.x

Staples, M., Marks, R., & Giles, G. (1998). Trends in the incidence of Non-Melanocytic Skin Cancer (NMSC) treated in Australia 1985–1995: Are primary prevention programs starting to have an effect? *International Journal of Cancer*, *78*(2), 144–148. https://doi.org/10.1002/(sici)1097-0215(19981005)78:2<144::aid-ijc3>3.0.co;2-z

Torres, V., Herane, M. I., Costa, A., Martin, J. P., & Troielli, P. (2017). Refining the ideas of "ethnic" skin. *Anais Brasileiros de Dermatologia*, *92*(2), 221–225. https://doi.org/10.1590/abd1806-4841.20174846

Trakatelli, M., Bylaite-Bucinskiene, M., Correia, O., Cozzio, A., De Vries, E., Medenica, L., et al. (2017). Clinical assessment of skin phototypes: Watch your words. *European Journal of Dermatology*, *27*(6), 615–619. https://doi.org/10.1684/ejd.2017.3129

Udelhofen, P. M., Gies, P., Roy, C., & Randel, W. J. (1999). Surface UV radiation over Australia, 1979–1992: Effects of ozone and cloud cover changes on variations of UV radiation. *Journal of Geophysical Research*, *104*(D16), 19135–19159. https://doi.org/10.1029/1999JD900306

Ulpiani, G., Ranzi, G., & Santamouris, M. (2020). Experimental evidence of the multiple microclimatic impacts of bushfires in affected urban areas: The case of Sydney during the 2019/2020 Australian season. *Environmental Research Communications*, *2*(6), 065005. https://doi.org/10.1088/2515-7620/ab9e1a

UNEP. (2020). The Montreal protocol on substances that deplete the ozone layer. Retrieved from https://ozone.unep.org/treaties/montreal-protocol

U.S. Census Bureau. (2019). *2018 national population projections tables: Race and Hispanic Origin by Age Group*. U.S. Census Bureau.

U.S. EPA. (2020). *Updating the atmospheric and health effects framework model: Stratospheric ozone protection and human health benefits*. U. S. E. P. Agency Ed.

van Dijk, A., Slaper, H., den Outer, P. N., Morgenstern, O., Braesicke, P., Pyle, J. A., et al. (2013). Skin cancer risks avoided by the Montreal protocol—worldwide modeling integrating coupled climate-chemistry models with a risk model for UV. *Photochemistry and Photobiology*, *89*(1), 234–246. https://doi.org/10.1111/j.1751-1097.2012.01223.x

Wenny, B., Schafer, J., DeLuisi, J., Saxena, V., Barnard, W., Petropavlovskikh, I., & Vergamini, A. (1998). A study of regional aerosol radiative properties and effects on ultraviolet-b radiation. *Journal of Geophysical Research*, *103*(D14), 17083–17097. https://doi.org/10.1029/98jd01481

West, S. K., Longstreth, J. D., Munoz, B. E., Pitcher, H. M., & Duncan, D. D. (2005). Model of risk of cortical cataract in the US population with exposure to increased ultraviolet radiation due to stratospheric ozone depletion. *American Journal of Epidemiology*, *162*(11), 1080–1088. https://doi.org/10.1093/aje/kwi329

WMO. (2018). *Scientific assessment of ozone depletion: 2018*. World Meteorological Organization.

WMO. (2022). *Scientific assessment of ozone depletion: 2022*. World Meteorological Organization.

Yang, X., Zhao, C., Yang, Y., & Fan, H. (2021). Long-term multi-source data analysis about the characteristics of aerosol optical properties and types over Australia. *Atmospheric Chemistry and Physics*, *21*(5), 3803–3825. https://doi.org/10.5194/acp-21-3803-2021

Zhang, H., Wang, J., Castro García, L., Zeng, J., Dennhardt, C., Liu, Y., & Krotkov, N. A. (2019). Surface erythemal UV irradiance in the continental United States derived from ground-based and OMI observations: Quality assessment, trend analysis and sampling issues. *Atmospheric Chemistry and Physics*, *19*(4), 2165–2181. https://doi.org/10.5194/acp-19-2165-2019

Zhang, W., Zeng, W., Jiang, A., He, Z., Shen, X., Dong, X., et al. (2021). Global, regional and national incidence, mortality and disability-adjusted life-years of skin cancers and trend analysis from 1990 to 2019: An analysis of the global Burden of disease study 2019. *Cancer Medicine*, *10*(14), 4905–4922. https://doi.org/10.1002/cam4.4046